Manipulating Molecular Transport Through Nanoporous Membranes by Control of Electrokinetic Flow: Effect of Surface Charge Density and Debye Length

ARTICLE *in* LANGMUIR · SEPTEMBER 2001

Impact Factor: 4.46 · DOI: 10.1021/la010429j

4 AUTHORS, INCLUDING:

Jonathan Sweedler
University of Illinois, Urbana-Champaign
510 PUBLICATIONS **15,042** CITATIONS

SEE PROFILE

Manipulating Molecular Transport through Nanoporous Membranes by Control of Electrokinetic Flow: Effect of Surface Charge Density and Debye Length

Tzu-Chi Kuo, Lisa A. Sloan, Jonathan V. Sweedler,* and Paul W. Bohn*

Department of Chemistry and Beckman Institute for Advanced Science and Technology, University of Illinois at Urbana-Champaign, 600 South Mathews, Urbana, Illinois 61801

Received March 22, 2001. In Final Form: July 13, 2001

Molecular transport through nanoporous nuclear-track-etched membranes was investigated with fluorescent probes by manipulating applied electric field polarity, pore size, membrane surface functionality, pH, and the ionic strength. Three forces contribute to analyte transport through membranes: ion migration, electroosmosis, and diffusion. Diffusion dominates under field-free conditions with surface hydrophobicity controlling solvent access to the nanochannels and hence the magnitude of transport by diffusion. In low ionic strength solutions ($\mu \sim 10$ mM), electroosmosis dominates transport when the membranes are biased, and the charge state of the surface determines the direction of flow. At high ionic strength ($\mu \sim 1$ M), ion migration dominates in hydrophobic membranes, and diffusion is controlling in hydrophilic membranes. The magnitude and polarity of the interior surface charge is controlled by surface functionality and displays the largest impact on molecular transport. The analyte can migrate in opposite directions under the same applied electric field by modifying either membrane surface charge or solution ionic strength. Transport can be fine-tuned by adjusting pH under low ionic strength conditions in either type of membrane. Increasing the surface charge density, σ_s, enhances the mobile counterion concentration, increasing the electroosmotically driven flux. Comparisons of behavior under different conditions are understood by reference to the product, κa, of the inverse Debye length, κ, and the pore diameter, a.

Introduction

The overwhelming success of efforts to develop microelectromechanical systems (MEMS) has resulted in a plethora of devices and functions in which fluidic processing of molecular and biomolecular elements occurs in structures of micrometer characteristic dimensions. The concept of miniaturizing a complete analytical system (μ-TAS) started with the work of Terry et al. who fabricated a complete gas chromatography system on a silicon wafer.[1] More than a decade later, Manz and co-workers established another milestone in μ-TAS by demonstrating liquid-phase separations,[2] a development which catalyzed contributions from a number of laboratories.[3−8] Since then, there has been explosive growth in research in the field, including advances in fabrication methods for silicon[9] optically transparent materials and advances in polymer substrates[10−15] and the development of rapid prototyping in poly(dimethylsiloxane) (PDMS),[14,15] and much effort has gone into component development, including mixers, valves, interconnects, filters, and other elements required for a complete microfluidics system.[16−19]

The natural extension of these pioneering developments in microfluidic transport would extend capabilities to structures of nanometer characteristic dimensions. Active control over molecular transport at nanometer dimensions would comprise an enabling technology by permitting (a) new approaches to molecular separations which augment passive analyte−stationary phase interactions; (b) the study of reactions in which one or more reagents are available in limited quantities; and (c) coupling of powerful methods of molecular identification, for example, mass spectrometry, to spatially and temporally resolved molecular sampling methods, that is, preparative chromatography on unprecedented low levels of analyte. Thus, there is ample motivation to explore molecular transport in nanoscale structures. It is especially interesting to consider the potential applications of nanofluidic structures as interconnects between microfluidic channels.

* To whom correspondence should be addressed. Phone: 217-333-0676 (Bohn); 217-244-4759 (Sweedler). Fax: 217-244-8068. E-mail: bohn@scs.uiuc.edu; sweedler@scs.uiuc.edu.

(1) Terry, S. C.; Jerman, J. H.; Angell, J. B. *IEEE Trans. Electron Devices* **1979**, *ED-26*, 1880−1886.
(2) Manz, A.; Graber, N.; Widmer, H. M. *Sens. Actuators, B* **1990**, *1*, 244−248.
(3) Harrison, D. J.; Fluri, K.; Seiler, K.; Fan, Z.; Effenhauser, C. S.; Manz, A. *Science* (*Washington, D.C.*) **1993**, *261*, 895−897.
(4) Seiler, K.; Fan, Z. H. H.; Fluri, K.; Harrison, D. J. *Anal. Chem.* **1994**, *66*, 3485−3491.
(5) Jacobson, S. C.; Hergenroder, R.; Koutny, L. B.; Warmack, R. J.; Ramsey, J. M. *Anal. Chem.* **1994**, *66*, 1107−1113.
(6) Jacobson, S. C.; McKnight, T. E.; Ramsey, J. M. *Anal. Chem.* **1999**, *71* (1), 4455−4459.
(7) Woolley, A. T.; Mathies, R. A. *Proc. Natl. Acad. Sci. U.S.A.* **1994**, *91*, 11348−11352.
(8) Haab, B. B.; Mathies, R. A. *Anal. Chem.* **1999**, *71*, 5137−5145.
(9) Christel, L. A.; Petersen, K.; McMillan, W.; Kovacs, G. T. A. In *Technical Digest of the 1998 Solid-State Sensor and Actuator Workshop*; Transducers Research Foundation: Cleveland, OH, 1998; pp 363−366.
(10) Folch, A.; Ayon, A.; Hurtado, O.; Schmidt, M. A.; Toner, M. *J. Biomech. Eng.* **1999**, *121*, 28−34.
(11) Becker, H.; Gartner, C. *Electrophoresis* **2000**, *21*, 12−26.
(12) Lee, L. P.; Berger, S. A.; Liepmann, D.; Pruitt, L. *Sens. Actuators, A* **1998**, *71*, 144−149.
(13) Martin, P. M.; Matson, D. W.; Bennett, W. D.; Hammerstrom, D. J. *Proc. SPIE-Int. Soc. Opt. Eng.* **1998**, *3515*, 172−176.
(14) Duffy, D. C.; Schueller, O. J. A.; Brittain, S. T.; Whitesides, G. M. *J. Micromech. Microeng.* **1999**, *9*, 211−217.
(15) McDonald, J. C.; Duffy, D. C.; Anderson, J. R.; Chiu, D. T.; Wu, H. K.; Schueller, O. J. A.; Whitesides, G. M. *Electrophoresis* **2000**, *21*, 27−40.
(16) Koch, M.; Schabmueller, C. G. J.; Evans, A. G. R.; Brunnschweiler, A. *Sens. Actuators, A* **1999**, *74*, 207−210.
(17) Jaeggi, D.; Gray, B. L.; Mourlas, N. J.; van Drieenhuizen, B. P.; Williams, K. R.; Maluf, N. I.; Kovacs, G. T. A. In *Technical Digest of the 1998 Solid-State Sensor and Actuator Workshop*; Transducers Research Foundation: Cleveland, OH, 1998; pp 112−115.
(18) Man, P. F.; Mastrangelo, C. H.; Burns, M. A.; Burke, D. T. In *Proceedings, IEEE Micro Electro Mechanical Systems, 11th*; Institute of Electrical and Electronics Engineers: New York, 1998; pp 45−50.
(19) Yang, X.; Yang, J. M.; Tai, Y.-C.; Ho, C.-M. *Sens. Actuators, A* **1999**, *73*, 184−191.

10.1021/la010429j CCC: $20.00
Published on Web 09/08/2001

Nanofluidic interconnects mediating flow in the 10−100 nm size regime can potentially achieve digital transfer of fluids between microfluidic channels in which the interconnect itself is integral to the controlled movement of molecules.

Nuclear-track-etched (e.g., Nuclepore) membranes, used in size-based filtration applications,[20−24] have attracted attention as model systems for studying electrokinetic flow in cylindrical channels.[25−30] Surface charge density, σ_s, is a critically important property influencing these phenomena,[31,32] because the enhanced surface area to volume ratio (A_s/V) at nanometer dimensions means that a significant fraction of the total charge is bound to the walls and is immobile. It determines the magnitude of the surface potential and the applicability of the Debye−Hückel approximation, and ultimately it provides an experimental handle to adjust the microscopic processes which determine transport in the channel. Significant effort has been made to understand the role of surface potential and how the chemical makeup of the interior surfaces of nanofluidic channels can control molecular transport. Following the seminal discovery by Martin et al. that ion permselective membranes can be obtained using electroless Au-coated channels in nuclear-track-etched membranes,[33] several groups have explored the use of electroless Au deposition followed by self-assembly to fabricate structures which can mediate molecular transport.[34−38]

While some significant issues arise when considering fluid flow or chemical reactivity in micrometer-scale structures, especially near surfaces or container walls, a significant fraction of the structure can often be treated as though it were macroscopic. In contrast, fluid flow and chemical reactions which occur in structures with nanometer characteristic dimensions are fundamentally different, because the characteristic length scales which describe important physicochemical phenomena are approximately equal to the dimensions of the devices in which they occur. The most obvious example is that the Debye length, κ^{-1}, which characterizes the length scale of ionic interactions in solution can be made to span the range 1 nm $\leq \kappa^{-1} \leq$ 50 nm by adjusting the ionic strength of a buffer solution in the high-to-low mM concentration range. Thus, it is possible to run experiments under conditions ranging from those where the electrical double layer is wall-confined to conditions where the double layer extends well out into the channel. Given the potential of these membranes for important technological applications, especially their potential to act as intelligent interconnects, we are interested in understanding how the various aspects of the interior surface composition of nanochannel membranes contribute to control molecular transport.

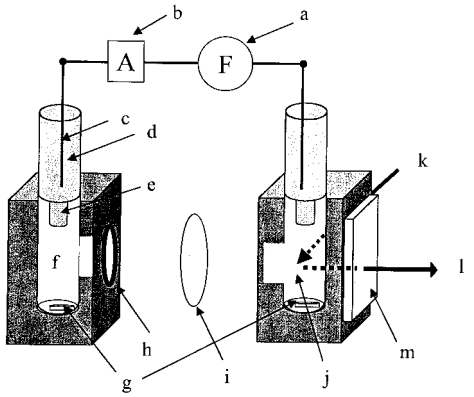

Figure 1. Schematic diagram of the bicell used for membrane transport measurements: (a) function generator, (b) amperometer, (c) Pt wire, (d) 3 M KCl electrolyte solution, (e) glass frit, (f) source side, (g) magnetic stir bar, (h) O-ring, (i) nanoporous membrane, (j) receiving side, (k) 488 nm excitation, (l) fluorescence emission, and (m) fused silica plates attached to three faces of the cell, through which fluorescence intensity is monitored.

Experimental Section

Materials. Deionized H_2O (18.2 MΩ cm) from a Milli-Q UV-Plus system (Millipore) was used to prepare all solutions. The fluorescent probe fluorescein (disodium salt, Sigma) was used as received. Nucleopore polycarbonate track etched (PCTE) and poly(vinylpyrrolidone)-free (PVPF) membranes were purchased from Fisher and stored under dry N_2 prior to use. Both membrane varieties (PCTE and PVPF) were 2.5 cm in diameter and 6−10 μm thick, depending on pore size. Hydrophilic PCTE membranes with pore diameters a = 15 or 200 nm were used, both having highly monodisperse distributions of pores with pore densities 3×10^8 cm$^{-2} < N_p < 6 \times 10^8$ cm^{-2}, depending on pore diameter. PVPF membranes with a = 220 nm with specifications comparable to that of 200 nm PCTE were also used for comparison. Notably, the PVPF membranes are hydrophobic. Phosphate buffer solutions (PBS, pH = 7, 8, 11) were prepared from mono-, di-, and tribasic potassium phosphate salts in 5 and 500 mM concentrations. Ionic buffers were prepared by adding aliquots of 1 M $KCl_{(aq)}$ to the PBS buffers until solution conductivity matched that of the most basic PBS solution.

Transport Measurements. The transport experiments were carried out in a standard membrane transport bicell. The membrane, held in place via an O-ring, served to separate the two identical compartments (2.5 mL capacity) in a custom-built cell made of Delrin (Figure 1). Magnetic stir bars were placed in both the source compartment (containing the fluorescent probe in PBS) and the receiving compartment (initially PBS only) and were rotated at a constant speed throughout the course of an experiment, to ensure effective mixing. The fluorescence signal from the receiving side was monitored with a fluorimeter (Spex) operating in 90° excitation/detection orientation, and control and data collection were achieved with a computer running a program under LabVIEW (National Instruments). Fluorescence working curves for Fl^{2-} were obtained at the pH values of interest at excitation and emission wavelengths of 488 and 516 nm, respectively, and used to convert the fluorescence intensities to fluorescein, Fl^{2-}, concentrations in the receiver compartment.

(20) Henry, J. D.; Lawler, L. F.; Kuo, C. H. A. *AIChE J.* **1977**, *23*, 851−859.
(21) Hernadez, A.; Martinez-Villa, F.; Ibanez, J. A.; Arribas, J. I.; Tejerina, A. F. *Sep. Sci. Technol.* **1986**, *21*, 665−677.
(22) Hope, M. J.; Bally, M. B.; Webb, G.; Cullis, P. R. *Biochim. Biophys. Acta* **1985**, *812*, 55−65.
(23) Wakeman, R. J.; Tarleton, E. S. *Chem. Eng. Res. Des.* **1991**, *69*, 386−397.
(24) Nystrom, M.; Lindstrom, M.; Matthiasson, E. *Colloids Surf.* **1989**, *36*, 297−312.
(25) Rice, C. L.; Whitehead, R. *J. Phys. Chem.* **1965**, *69*, 4017−4024.
(26) Anderson, J. L.; Koh, W.-H. *J. Colloid Interface Sci.* **1977**, *59*, 149−158.
(27) Westermann-Clark, G. B.; Anderson, J. L. *J. Electrochem. Soc.* **1983**, *130*, 839−847.
(28) Ibanez, J. A.; Forte, J.; Hernandez, A.; Tejerina, F. *J. Membr. Sci.* **1988**, *36*, 45−54.
(29) Brendler, E.; Ratkje, S. K.; Hertz, H. G. *Electrochim. Acta* **1996**, *41*, 169−176.
(30) Wan, Q. H. *Anal. Chem.* **1997**, *69*, 361−363.
(31) Fair, J. C.; Osterle, J. F. *J. Chem. Phys.* **1971**, *54*, 3307−3316.
(32) Martinez, L.; Gigosos, M. A.; Hernandez, A.; Tejerina, F. *J. Membr. Sci.* **1987**, *35*, 1−20.
(33) Nishizawa, M.; Menon, V. P.; Martin, C. R. *Science* (*Washington, D.C.*) **1995**, *268*, 700−702.
(34) Hulteen, J. C.; Jirage, K. B.; Martin, C. R. *J. Am. Chem. Soc.* **1998**, *120*, 6603−6604.
(35) Jirage, K. B.; Hulteen, J. C.; Martin, C. R. *Anal. Chem.* **1999**, *71*, 4913−4918.
(36) Ito, Y.; Park, Y. S.; Imanishi, Y. *Langmuir* **2000**, *16*, 5376−5381.
(37) Hou, Z.; Abbott, N. L.; Stroeve, P. *Langmuir* **1998**, *14*, 3287−3297.
(38) Hou, Z.; Abbott, N. L.; Stroeve, P. *Langmuir* **2000**, *16*, 2401−2404.

The pK_2 for fluorescein is 6.43,[39] so Fl^{2-} is the predominant species at pH ≥ 7. Therefore, throughout the paper the fluorescent probe is referenced as Fl^{2-}, although near neutral pH it exists as a mixture of Fl^{2-} and the protonated HFl^{-}. The limit of detection for Fl^{2-} in this system configuration was 200 pM at pH 7. The initial concentration of Fl^{2-} on the source side was 1 μM in PBS, unless otherwise noted. In experiments conducted with the 15 nm pore diameter PCTE membranes, the probe concentration in the source side decreased less than 5% during a typical transport experiment. However, the same constraint did not apply to most experiments with 200 nm membranes, since diffusion has a greater effect with the larger pore size hydrophilic membranes. Fresh membranes (PCTE or PVPF) and solutions were used for each trial.

Potentials were applied across the membrane junction via Pt electrodes ($Pt_{(s)}$/3 M $KCl_{(aq)}$) stabilized atop the source and receiving compartments. A function generator (Hewlett-Packard, model 8116A) supplied the 1-kHz ac sinusoidal wave (4 V peak-to-peak) and dc offset (±14 V). The ac signal was originally used to study the diffusion behavior under zero dc offset and is retained here for consistency with earlier control experiments; however, it is not essential for experiment conditions reported here. No significant differences were observed between experiments with and without ac excitation. The electrode on the source side was connected to ground, and applied voltages are given throughout as $V_{rec} - V_{source}$. The applied voltage and current were both monitored during the course of each experiment. To ensure solution filling of pores, before each transport run the membrane was conditioned with buffer solution in both half cells under ±14 V_{rms} for 5 min total; then, the buffer in the source side was replaced with fluorescein solution. Most permeation experiments were conducted with the same temporal program of dc offsets: 0−20 min, 0 V; 20−30 min, + bias; 30−35 min, 0 V; 35−45 min, − bias; and 45−50 min, 0 V. Different sequences of applied electric field were used on various occasions, but no significant differences in qualitative behavior were observed. For clarity, the bias which causes an increase of fluorescent intensity on the receiving side is defined as forward bias, and the opposite situation is defined as reverse bias.

To compare the effect of applied voltage on transport, the average Fl^{2-} flux was calculated for the experimental intervals 8−18, 23−28, and 38−42 min, corresponding to the diffusion, positive polarization, and negative polarization periods, respectively. These intervals were chosen to ensure that estimates of Fl^{2-} flux were obtained at steady state, since the system typically required several minutes to stabilize in response to the change in applied bias. J_{off}, J_+, and J_- represent measured Fl^{2-} fluxes in the diffusion, positive polarization, and negative polarization periods, respectively; the ratios among J_+, J_-, and J_{off} are used to measure how transport is enhanced or inhibited in response to the applied field. Since there are numerous parameters, including membrane thickness, channel diameter, surface charge density, axial variation of the radial cross section, and so forth, which together determine the absolute flux, only relative flux values are used.

Results and Discussion

Large Debye Length Limit. Both 15 and 200 nm pore diameter membranes were used to investigate flux as a function of pH and pore diameter (Figures 2 and 3). Each experiment began by holding the membrane in field-free conditions for a period of time to judge the importance of diffusive transport. PCTE membranes are manufactured with a poly(vinylpyrrolidone) (PVP) surface coating which renders them hydrophilic. The amine N atom of PVP may be protonated to establish a positive surface charge, so the surface charge density, σ_s, is largest at the lowest solution pH values, yielding positive interior wall charges for solutions at pH 7 and 8 and a more neutral surface for pH 11. Typically, for hydrophilic PCTE membranes the Fl^{2-} probe concentration in the receiving chamber increased as Fl^{2-} ions diffused from the more concentrated source region. Under positive applied potentials, the flux, that is, the slope of the [Fl^{2-}] versus time plot, of Fl^{2-} ions increased and returned to a level similar to the first field-free period when the voltage was removed. When a negative voltage was applied, transport was inhibited, as indicated by a near-zero flux under these conditions. Comparing results among experiments conducted with identical pore size PCTE membranes, smaller fluxes were observed at higher pH under positive external voltage. This pH-dependent transport is clearly correlated with changes in the surface charge density on the interior nanopore wall, with the most highly charged interior channels, formed at the lowest pH, corresponding to the largest forward-biased probe fluxes, cf. Figure 2. The other possible cause for pH-dependent transport is the ratio of [HFl^{-}]/[Fl^{2-}] at different pH, which decreases from 0.27 at pH 7 to 0.027 at pH 8. Under positive bias, the net fluorescein ion migration rate at pH 7 should be smaller than that at pH 8 based on their net charges; however, the net flux, J_+, is higher at pH 7 than at pH 8 and 11, consistent with the fact that electroosmosis dominates the flux through PCTE membranes at 5 mM PBS.

On the basis of the pore diameters and densities, the pore area as a fraction of total membrane area is 9.4% for 200 nm PCTE and 0.11% for 15 nm PCTE. These ratios

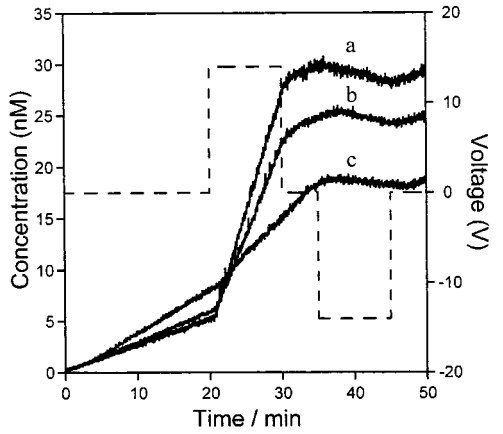

Figure 2. Field-induced permeation of Fl^{2-} in a 15 nm pore diameter PCTE membrane in 5 mM PBS at pH 7 (a), 8 (b), and 11 (c). The applied dc offset potential program is referenced to the right ordinate. Fl^{2-} concentration in the receiving compartment is referenced to the left ordinate.

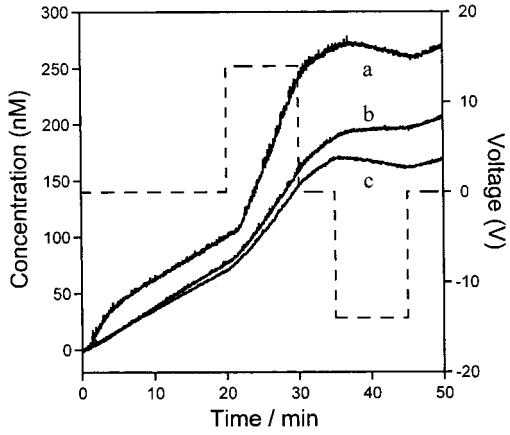

Figure 3. Field-induced permeation of Fl^{2-} in a 200 nm pore diameter PCTE membrane in 5 mM PBS at pH 7 (a), 8 (b), and 11 (c). The applied dc offset potential program is referenced to the right ordinate. Fl^{2-} concentration in the receiving compartment is referenced to the left ordinate.

(39) Sjöback, R.; Nygren, J.; Kubista, M. *Spectrochim. Acta, Part A* **1995**, *51*, L7−L21.

Table 1. Flux of Fl^{2-} through Polycarbonate Membranes under Varying Field and Electrolyte Concentrations

[PBS]	type of membrane	pH	J_{off}[a]	J_+	J_+/J_{off}	J_-	J_-/J_{off}
5 mM	15 nm PCTE	7	0.25 (1.0)[b]	2.32 (0.6)	9.10	−0.14 (15.8)	−0.55
		8	0.30 (0.5)	1.73 (0.9)	5.75	−0.16 (6.0)	−0.53
		11	0.43 (0.5)	0.71 (1.3)	1.67	−0.09 (13.6)	−0.20
	200 nm PCTE	7	3.83 (0.5)	16.54 (0.9)	4.32	−1.50 (4.3)	−0.39
		8	4.02 (0.3)	8.83 (0.7)	2.20	0.42 (8.3)	0.10
		11	3.56 (0.2)	8.04 (0.5)	2.26	−0.96 (4.3)	−0.27
	220 nm PVPF	7	0.00 (12.3)	0.02 (7.0)	4.94	0.49 (1.0)	96.33
		8	0.03 (1.8)	0.02 (13.0)	0.57	2.54 (0.6)	93.62
		11	0.01 (3.8)	0.00 (113)	−0.11	4.79 (0.4)	335.10
500 mM	15 nm PCTE	7	0.65 (0.6)	1.23 (1.2)	1.90	0.15 (11.5)	0.23
		8	0.45 (0.5)	0.94 (1.6)	2.09	0.03 (33.9)	0.07
		11	0.31 (0.8)	0.60 (1.8)	1.94	0.13 (13.3)	0.41
	200 nm PCTE	7	3.44 (0.8)	3.78 (1.4)	1.10	2.00 (2.6)	0.58
		8	3.66 (0.4)	4.62 (0.9)	1.26	2.16 (1.8)	0.59
		11	4.43 (0.4)	4.21 (1.4)	0.95	4.32 (2.2)	0.97
	220 nm PVPF	7	0.01 (9.3)	0.50 (1.0)	68.87	0.05 (14.4)	7.12
		8	0.01 (3.8)	0.47 (0.9)	49.01	0.02 (25.6)	2.08
		11	0.0019 (18.3)	0.038 (4.1)	20.28	0.0081 (47.9)	4.24

[a] J in nM/min. [b] Values in parentheses are standard deviations in percentage.

would suggest the ratio of field-free fluxes between 15 nm and 200 nm PCTE to be 1:85, but the measured ratio in the diffusion region, J_{off}, from Table 1, is only ∼1:10. Schonenberger et al. reported cigarlike channel shapes of metal nanowires grown in PCTE membrane pores, showing that channel diameters are almost 3 times larger near the centers than on the membrane surface.[40] If this geometric factor is taken into account in the calculation of resistance, the ratio 1:85 becomes 1:28, which is still significantly larger than 1:10. This discrepancy can be ascribed to the electrostatic interaction of the negatively charged Fl^{2-} with the positively charged pore surface, the magnitude of interaction decreasing as the pore diameter increases, generating a larger effect for smaller pore diameters and resulting in a smaller increase in flux with pore diameter than would be predicted on the basis of pore diameter alone. This observation agrees with several previous studies, which demonstrate that electrostatic attraction enhances the transport while repulsion inhibits it.[41−43] The effective diffusion rate in the pore might also be expected to decrease as pH increases since the PCTE surface changes from positively charged to neutral causing less electrostatic interaction between the Fl^{2-} and the wall. However, this trend is not observed, presumably because the perturbation in the magnitude of σ_s is much smaller than the perturbation associated with reversing the sign of the wall charge. Clearly, pH-related changes in the charge state of the surface cause more pronounced effects during the field-on periods, through the impact they have on electroosmosis, than in the field-free periods.

Unlike PCTE, PVPF membranes are not post-etch treated with PVP, leaving the exposed surface both relatively hydrophobic and negatively charged. The hydrophobic nature of PVPF plays an important role in transport in the field-free diffusion region. In contrast to the behavior observed with the PCTE membranes, there was no significant Fl^{2-} flux in either field-free or positively biased periods, but a large pH-dependent flux was observed after application of a negative bias (Figure 4). Extremely high J_-/J_{off} ratios were obtained in these PVPF

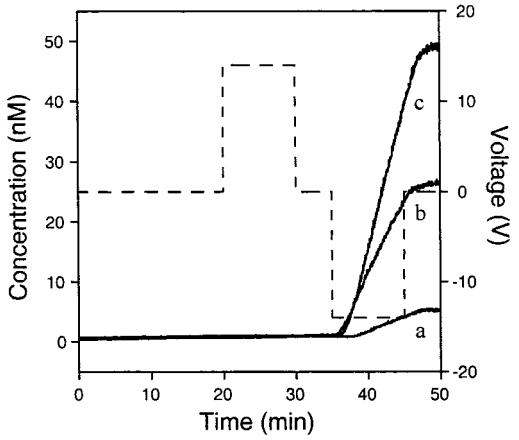

Figure 4. Field-induced permeation of Fl^{2-} in a 220 nm pore diameter PVPF membrane in 5 mM PBS at pH 7 (a), 8 (b), and 11 (c). The applied dc offset potential program is referenced to the right ordinate. Fl^{2-} concentration in the receiving compartment is referenced to the left ordinate.

membranes, due principally to the near-zero transport in the field-off period ($J_{off} \sim 0$). The quantitative flux ratios thus contain a relatively large error due to the uncertainty in J_{off}, but the trend is important. In contrast to transport in PCTE membranes, PVPF membranes are forward-biased under negative applied potential, and since the only difference between the membranes is the charge imparted by the surface coating, it is reasonable to ascribe the varying behavior to the polarity of the surface charge. The PVPF membrane surface either is uncharged or carries a small negative σ_s at neutral pH, but it becomes more negative as the solution is made more basic. Given the need for mobile cations to balance the immobile wall-based charge, the polarity of forward- and reverse-bias conditions is reversed. The Fl^{2-} flux in PVPF membranes under forward (negative) bias conditions is much larger than under reverse (positive) bias or field-free conditions. As pH increases, J_- increases, consistent with the formation of a negatively charged surface with a larger σ_s capable of inducing greater electroosmotic flow. However, as shown in Table 1, J_- measured for 220 nm pore diameter PVPF membranes is still significantly smaller than J_+ from 200 nm PCTE. The slower transport in PVPF membranes can be attributed to two effects: (1) hydrophobicity of the PVPF surface limits access of the aqueous solution to the pores, reducing the effective pore size, and (2) J_+ of PCTE results from the vector addition of electroosmotic, J_{eo}, and ion

(40) Schonenberger, C.; vanderZande, B. M. I.; Fokkink, L. G. J.; Henny, M.; Schmid, C.; Kruger, M.; Bachtold, A.; Huber, R.; Birk, H.; Staufer, U. *J. Phys. Chem. B* **1997**, *101*, 5497−5505.

(41) Bluhm, E. A.; Bauer, E.; Chamberlin, R. M.; Abney, K. D.; Young, J. S.; Jarvinen, G. D. *Langmuir* **1999**, *15*, 8668−8672.

(42) Bluhm, E. A.; Schroeder, N. C.; Bauer, E.; Fife, J. N.; Chamberlin, R. M.; Abney, K. D.; Young, J. S.; Jarvinen, G. D. *Langmuir* **2000**, *16*, 7056−7060.

(43) Lee, S.-B.; Martin, C. R. *Anal. Chem.* **2001**, *73*, 768−775.

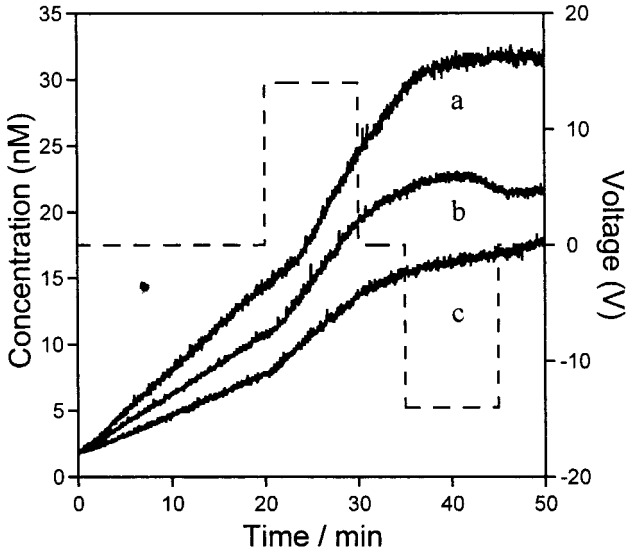

Figure 5. Field-induced permeation of Fl^{2-} in a 15 nm pore diameter PCTE membrane in 500 mM PBS at pH 7 (a), 8 (b), and 11 (c). The applied dc offset potential program is referenced to the right ordinate. Fl^{2-} concentration in the receiving compartment is referenced to the left ordinate.

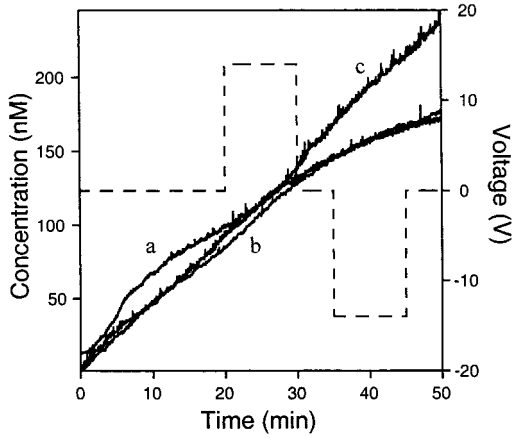

Figure 6. Field-induced permeation of Fl^{2-} in a 200 nm pore diameter PCTE membrane in 500 mM PBS at pH 7 (a), 8 (b), and 11 (c). The applied dc offset potential program is referenced to the right ordinate. Fl^{2-} concentration in the receiving compartment is referenced to the left ordinate.

migration, J_{im}, fluxes, while J_- of PVPF is the resultant of oppositely directed J_{im} and J_{eo} fluxes. The first of these effects is consistent with the ~0 flux observed in the field-free periods, and the second follows from considering the polarity of the probe and mobile counterions.

Small Debye Length Limit. Initially, 0.5 M PBS solutions were prepared as ionic strength buffers, which required a large amount of $KCl_{(s)}$, resulting in high Cl^- concentration in the buffer. The Fl^{2-} emission profile was altered when membranes were operated in this type of buffer, possibly because Cl^- interacts with the positively charged surface moieties resulting in the liberation of a surface component with fluorescent emission at 535 nm, which interferes with the measurement of the Fl^{2-} emission. To avoid this problem with probe signal interpretation, all subsequent experiments involving high-concentration buffers were performed without the addition of an ionic strength buffer.

As illustrated in Figures 5 and 6, the applied voltage had less effect on transport at high ionic strength than it did at lower ionic strength, especially with the larger (200 nm) pore size PCTE membrane, where no statistically

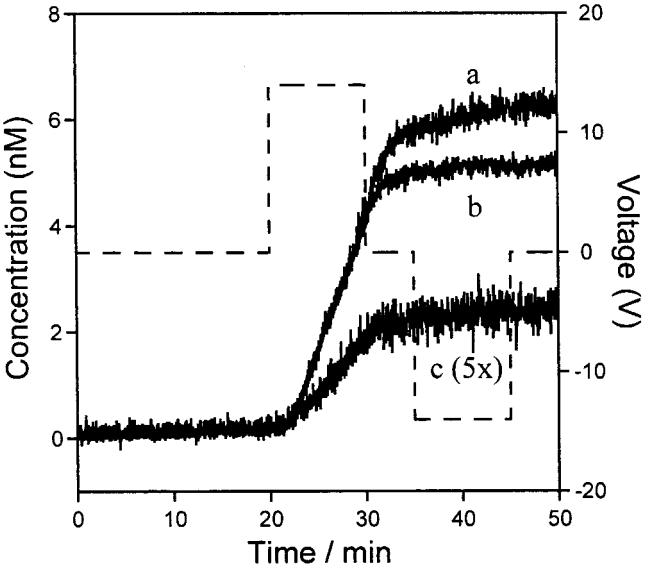

Figure 7. Field-induced permeation of Fl^{2-} in a 220 nm pore diameter PVPF membrane in 500 mM PBS at pH 7 (a), 8 (b), and 11 (c). The applied dc offset potential program given by the rectangular pulses is referenced to the right ordinate. Fl^{2-} concentration in the receiving compartment is referenced to the left ordinate. Note that curve c is amplified by 5×.

significant field-induced change in flux could be ascertained. For 15 nm pore diameter PCTE, the diffusive flux J_{off} was similar to that in 5 mM buffer. Positive bias increased the flux, and negative bias decreased it, but J_+/J_{off} was only ~2 at all pH values, compared to values of ~7 for 5 mM PBS at pH 7. Also in contrast to the low ionic strength case, the magnitude of the Fl^{2-} flux was independent of pH. Although the J_+/J_{off} ratios were small and similar for all pH values used, the ratio was not 1, and there was still an inflection in the slope showing some degree of external bias control with 15 nm PCTE in 0.5 M PBS. For 200 nm pore diameter PCTE, not only was the pH dependence of the flux diminished but so was the effect of external bias, viz., Figure 6. An electrostatic effect can barely be discerned in diminishing the flux slightly under reverse (negative) bias compared to the flux under forward bias or in the field-free period. Depletion of probe from the source reservoir could result in slower transport rates over time in the 200 nm PCTE membranes, but it would not account for the lack of an effect when positive bias was applied. Also, there were differences in conductivity among different pH buffers, but the buffer conductivity did not correlate with measured flux and so cannot explain the small differences in flux.

When 0.5 M PBS solutions were used with 220 nm PVPF (Figure 7), a significant increase in transport was observed under positive bias, while transport during negative bias and during the field-free period was indistinguishable from zero. This result was not expected based on the polarity of the surface charge (negative). As in the 200 nm PCTE membrane, electroosmosis is not significant in the 220 nm PVPF case, leaving ion migration as the major force driving transport at high ionic strength. Therefore, the anion Fl^{2-} responded to ion migration (electrophoretic) forces produced by the positive bias to move toward the receiving side, even though electroosmosis would ostensibly drive transport in the opposite direction. The absolute magnitude of the flux in this case is small, of the order of J_{off} for the 15 nm PCTE membrane, so the effective pore size is still much smaller than its physical size even at high ionic strength.

Table 2. Debye Lengths, κa, and Effective Pore Cross Sections under Different Conditions

	$\mu = 1$ M						$\mu = 10$ mM					
	15 nm			200 nm			15 nm			200 nm		
charge z	κ^{-1}	κa	% pore cross section	κ^{-1}	κa	% pore cross section	κ^{-1}	κa	% pore cross section	κ^{-1}	κa	% pore cross section
1	0.43	34.9	11.14	0.43	466	0.86	4.30	3.49	81.78	4.30	46.5	8.41
2	0.21	69.8	5.65	0.21	932	0.43	2.15	6.98	49.10	2.15	93.0	4.25
3	0.14	104.7	3.78	0.14	1398	0.29	1.43	10.47	34.56	1.43	139.5	2.85

Transport Control in Nanometer Scale Structures. The Guoy−Chapman theory[44] of the electrical double layer is employed to elucidate the source of the behavior at different ionic strengths and pore diameters, a. Guoy−Chapman theory states that the thickness of the diffuse double layer, characterized by the Debye length, κ^{-1}, decreases as the electrolyte concentration increases, according to

$$\kappa^{-1} = [3.29zC^{1/2}]^{-1} \quad (1)$$

where κ^{-1} is in nm and C is the bulk z:z electrolyte concentration in mol/L. Table 2 shows the calculated double layer thickness and its percentage of the pore cross section under various conditions based on eq 1. κa in Table 2 is an index for how much the double layer thickness occupies the pore cross section. When $\kappa a \sim 1$, the electrical double layer extends over a significant fraction of the entire cross section, and electroosmosis dominates transport, since the counterions in the pores are evenly distributed throughout the pore volume.[45,46] When $\kappa a \gg 1$, the double layer becomes effectively confined near the walls, and electroosmosis contributes negligibly to transport; rather, ion migration and diffusion dominate.[30,47]

An examination of Table 2 reveals that the membranes and solution conditions used in this work can be classified into three operating regimes: (case 1) $\kappa a \sim 1$ as seen for 15 nm pore diameter at low ionic strength, (case 2) intermediate κa values ($15 \leq \kappa a \leq 150$) as obtained for 200 nm pores in 5 mM PBS or 15 nm pores at higher ionic strength (0.5 M PBS), and (case 3) $\kappa a \gg 1$ as obtained for large pores and high ionic strengths. Clearly, the extent to which electroosmosis dominates transport decreases with increasing κa. For case 1 conditions and a PCTE membrane, electroosmosis and ion migration both drive transport of the anionic probe, with positive potentials producing forward bias (Figure 2). The relative importance of electroosmosis compared to ion migration is seen from the pH dependence; increasing the wall charge increases the concentration of counterions, thereby enhancing the electroosmotic flux. Experiments performed under case 2 conditions in PCTE membranes show the same polarity electric field dependence as those performed with case 1 conditions, but the bias effect is much less pronounced. Indeed, a comparison of Figures 3 and 5 shows that the forward bias condition is the same and that forward bias fluxes are very similar. Notably, there is much less variation in flux with pH than was obtained under case 1 conditions (Figure 2). Previously, this laboratory reported that cationic, $DiIC_1(3)$ (1,1′,3,3,3′,3′-hexamethylindocarbocyanine iodide), and neutral, *d*-tryptophan, probes exhibited similar fluxes J_+ and J_- under case 2 conditions and at pH 7[47] confirming the importance of electroosmosis under case 2 conditions of κa. Case 3 behavior is obtained only for 200 nm PCTE in 500 mM PBS. Under these conditions, the electrical double layer is effectively collapsed, occupying <1% of the pore diameter in 200 nm PCTE membranes, and the electroosmotic contribution to transport is insignificant compared to diffusion and/or ion migration. For the hydrophilic PCTE membranes, diffusive transport is large, and the probe transport is not actively controlled by potential. Consistent with this observation, pH causes little variation in probe flux under case 3 conditions.

The same approach can be used to understand the behavior of PVPF membranes, if the hydrophobicity of the PVPF membranes is also considered. Because the membranes are hydrophobic, a diffusional barrier exists, so diffusion contributes negligibly to transport, and the competition is between electroosmosis (forward bias at negative applied potentials given the positive counterions) and ion migration (forward bias at positive applied potentials for the negatively charged Fl^{2-}) as can be seen by comparing Figures 4 and 7. Because the probe Fl^{2-} carries the opposite charge from the mobile counterions, H^+ and K^+, electroosmosis and ion migration work to move the probe in opposite directions allowing a very clean separation of the effects between low and high ionic strength. In comparing PVPF behavior to that of PCTE, it is useful to remember that the hydrophobicity of the membrane reduces the effective pore diameter. Thus, the experiments shown in Figure 4 are best considered as belonging to case 1, while those in Figure 7 belong to case 3. Comparing Figures 6 and 7 shows the relative importance of diffusion and ion migration in hydrophilic and hydrophobic membranes, respectively. Electroosmosis is negligible in both cases, but in Figure 6 transport in the hydrophilic PCTE membranes is dominated by diffusion, while diffusion is negligible for the PVPF membranes in Figure 7, thereby allowing the effect of ion migration to be clearly seen. These results demonstrate the potential of using nuclear-track-etched membranes to generate externally controllable molecular transport in structures of nanometer characteristic dimensions. We highlight the ability to engineer transport properties based on surface charge and structure (pore size and density) as well as fine-tune these properties based on solution composition (pH and ionic strength) and analyte properties (electrophoretic mobility).

Acknowledgment. This research was supported by the Department of Energy through Grant DE FG02 99ER62797, the Defense Advanced Research Projects Agency through Grant F30602-00-2-0567, and the National Cancer Institute through Grant PHS 1 R21 CA82081.

LA010429J

(44) Adamson, A. W. *Physical Chemistry of Surfaces*, 6th ed.; Wiley: New York, 1997.
(45) Schmid, G. *J. Membr. Sci.* **1998**, *150*, 151−157.
(46) Schmid, G. *J. Membr. Sci.* **1998**, *150*, 159−170.
(47) Kemery, P. J.; Steehler, J. K.; Bohn, P. W. *Langmuir* **1998**, *14*, 2884−2889.